31st Congress of the International Council of the Aeronautical Sciences

Belo Horizonte, Brazil; September 09-14, 2018

ACOUSTIC MODES AND GLOBAL INSTABILITIES IN WAKES AND JETS

Eduardo Martini* , **André Cavalieri*** , **Peter Jordan****
Instituto Tecnológico de Aeronáutica** , ****Université de Poitiers

Keywords: *Aeroacoustics, jet noise, flow instability*

Abstract

Unstable flows can be classified as absolutely unstable, when perturbations grow throughout the domain, and convectively unstable, where amplified perturbations are convected downstream, the flow locally returning to its equilibrium position. Absolute instabilities can be understood as a feedback loop, which can be long-ranged, as in impinging jets, or local, as in wakes and hot jets.

Local feed-back mechanism involves an upstream- and a downstream-traveling mode. It is well know in the literature that in sheared flows the latter is typically a Kelvin-Helmholtz mode; however little is found on the former. Inspired by recent findings in high Mach subsonic jets, that identified trapped acoustic waves in the jet core, we examine the role of such acoustic modes on the stability of jets and wakes.

Using a Double Vortex-Sheet (DVS) model, we derive conditions for which these flows behave as wave-guides, emulating acoustic ducts. We show that the upstream-traveling mode that leads to absolute instability is acoustic in essence, explaining differences in hot jets (symmetric) and cold wakes (antisymmetric) instabilities. Moreover, to evaluate the occurrence of such acoustic modes in turbulent flows, two-point correlations for a 0.4 Mach jet LES are constructed, highlighting that upstream influence in the flow is due to an acoustic mode.

This novel way to understand jet and wake instabilities can lead to novel control methods which can be used, for instance, to reduce aircraft noise and drag, and minimize cyclic loads in civil and maritime structures, and might be expanded as to explain other jet/wake behaviors, as instability trends with compressibility and with instability modes other then than Kelvin-Helmoltz.

1 Introduction

Sheared flows have been studied for decades, both due to their importance in applications such as on aeronautical, automotive, nautical and civil industries, as due to the diversity of behaviors that these flows exhibit. Instability waves known as Kelvin-Helmholtz (KH) modes are a key ingredient in understanding these behaviors, characterized by an amplification that is convected downstream, with growth rate and length scale of the perturbations scaling with the shear layers thickness.

The parallel flows assumption is widely used in order to simplify these problems, while keeping the key physical ingredients, as in Michalke's study of shear layer KH modes [1, 2] and Tam's study on three family of modes in supersonic jets [3].

In some non-parallel flows these unstable waves can be reflected by boundaries into an upstream mode, in some circumstances creating a feedback loop which leads to a general amplification of flow perturbations. Tonal noise in impinging jets [4, 5, 6, 7], is explained by KH waves being reflected as an acoustic wave by the plate. These waves travel upstream and are reflected again by the nozzle, re-exciting KH waves. A similar mechanism is also found on cavity flows [8, 9]. These "long-range" interactions are not

the only path to tonal noise or, as will be defined shortly, global instability.

Parallel flows can also exhibit local perturbation growth, created by short-range interactions. Huerre & Monkewitz [10] laid the framework for calculating and understanding these behaviors. He characterized the difference between absolute and convective stability, initially for parallel flows, and later for slowly divergent flows. The local, long time behavior of these flows are given by the dominant saddle point of the dispersion relation, where $d\omega/d\alpha = 0$ at α_0 and $\omega_0 = \omega(\alpha_0)$, where ω and α refer to frequency and streamwise wavenumber, respectively. If $\omega_{0,i} > 0$ the perturbations grow locally, and the flow is absolutely unstable. Otherwise the flow is either convective unstable, when perturbations grow but are convected downstream, and eventually all the flow returns to the equilibrium state, or stable, if there is no long term perturbation growth. The saddle point is marked by a "pinching" of upstream- and downstream-branches.

Absolute instability refers to the instability of parallel flows, or to the analysis of flow sections as if their where parallel, while global instability refers to the instability of general flows. An asymptotic analysis shows that a region with absolute instability is a necessary condition for global instabilities when the flow is slowly divergent [11], showing the usefulness of studding parallel flows in order to understand more complex configurations.

Towne et al. [12] used locally parallel analysis to explain the mechanisms behind Schimidt et al.'s [13] trapped jet modes as acoustic resonances in these flows. More recently, Jordan et al. [14] identified resonances conditions for jet-edge noise by studying which pairs of modes could be reflected by nozzle and edge forming a resonance.

A similar analysis can be performed for flows where "short-range" interactions lead to global instabilities. Both for wakes and hot jets, the downstream branch forming the saddle instability is identified as a KH mode. However the literature lacks an exploration of the upstream mode, even thought it is a necessary component of the instability. This paper comprises a study on the nature of these modes, and on their identification. We show that their essence is acoustic, and explore the necessary conditions for the occurrence of trapped acoustic waves within jets and wakes, which are then related to the flow stability. The different boundary conditions imposed by the vortex sheet on these modes explain the different symmetries found on cold wakes, with an antisymmetric pressure distribution, and hot jets, with a symmetric pressure distribution.

The article is organized as follows: Section 2 details the flow model, shows the solution of the linearized Euler equations and defines the Vortex-Sheet impedance. The conditions for which the flow behaves as a acoustic duct are explored in section 3 by analysis of vortex-sheet impedances. Limits for which hard- and soft-walled duct-like modes are present are identified, and their connection with global instabilities of incompressible jets and wakes demonstrated. Section 4 concludes the study by showing that acoustic-like modes are found on realistic flows, by identifying them on a 0.4 Mach LES database, described in [15], showing that the results previously obtained are not an artifact of the model used. Section 5 summarizes the results presented.

2 Acoustic Modes in the Double Vortex-Sheet Model

In order to capture the basic physical mechanisms of the flow, a double vortex sheet model (DVS) is used. The model consists of *inner* ($|y| < 1$) and *outer* ($|y| > 1$) regions.

In each domain an uniform flow is considered, with its own mean velocity ($U_{in,out}$), density ($\rho_{in,out}$), temperature ($T_{in,out}$) and sound speed ($a_{in,out}$). The flow profile is given by

$$U(y) = \begin{cases} U_{out} & ,|y| > 1 \\ U_{in} & ,|y| < 1 \end{cases}, \qquad (1)$$

with a similar expression for the other parameters. The model is illustrated in figure 1. The linearized Euler equations in each domain are

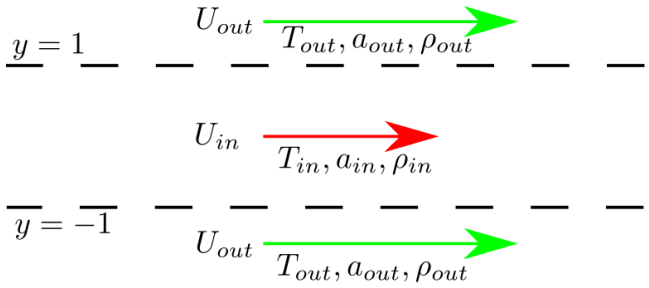

Fig. 1 Double Vortex-Sheet Model Illustration.

$$\left(\frac{\partial}{\partial t}+U_{in,out}\frac{\partial}{\partial x}\right)^2 p' = a_{in,out}^2\left(\frac{\partial^2}{\partial x^2}+\frac{\partial^2}{\partial y^2}\right)p', \tag{2}$$

where $p' = p'(x,y,t)$, with the corresponding mean flow and sound speed of each region.

As the problem is homogeneous in x and t, the *ansatz* $p'(x,y,t) = \hat{p}(y)e^{i(\alpha x-\omega t)}$ is used. The solutions in each domain are

$$\hat{p}(y) = \begin{cases} A_{in}\ e^{\xi_{in}\ y} + B_{in}\ e^{-\xi_{in}\ y} & ,|y|<1 \\ A_{out}e^{\xi_{out}y} + B_{out}e^{-\xi_{out}y} & ,|y|>1 \end{cases} \tag{3}$$

with

$$\xi_{in,out} = \sqrt{\alpha^2\left(1-\left(\frac{U_{in,out}-c}{a_{in,out}}\right)^2\right)}, \tag{4}$$

where $c = \omega/\alpha$ is the horizontal phase velocity, and branch cuts are chosen such that $-\pi/2 \leq \arg(\xi_{in,out}) < \pi/2$.

The exponentials on the *inner* and *outer* regions are then connected by interface conditions, which are given by the kinematic conditions and pressure continuity,

$$(-i\omega + iU_{in}\ \alpha)^2\hat{\eta}_\pm = -\frac{1}{\rho_{in}}\frac{\partial\hat{p}_{in}}{\partial y}(\pm1), \tag{5}$$

$$(-i\omega + iU_{out}\alpha)^2\hat{\eta}_\pm = -\frac{1}{\rho_{out}}\frac{\partial\hat{p}_{out}}{\partial y}(\pm1), \tag{6}$$

$$\hat{p}_{in}(\pm1) = \hat{p}_{out}(\pm1), \tag{7}$$

where $\eta_\pm$ is the displacement of the vortex sheet at $y = \pm1$.

Equations 4–7, with boundary condition $\hat{p}(\pm\infty) \to 0$, lead to the dispersion relations for antisymmetric and symmetric modes,

$$\tanh(\xi_{in}\ ) = -\frac{\rho_{in}}{\rho_{out}}\frac{\xi_{out}}{\xi_{in}}\left(\frac{c-U_{in}}{c-U_{out}}\right)^2, \tag{8}$$

$$\coth(\xi_{in}\ ) = -\frac{\rho_{in}}{\rho_{out}}\frac{\xi_{out}}{\xi_{in}}\left(\frac{c-U_{in}}{c-U_{out}}\right)^2. \tag{9}$$

Other flow perturbation components can be obtained as function of the pressure using

$$\hat{u}(y) = \frac{\hat{p}(y)}{(c-U)\rho}, \quad \hat{v}(y) = \frac{\frac{\partial\hat{p}}{\partial y}(y)}{i\alpha(c-U)\rho}. \tag{10}$$

A parametrization that allows for a continuous transition between jets and wakes is used,

$$\begin{aligned} U_{in} &= -V_{ref} & ,U_{out} &= 1-V_{ref}, \\ T_{in} &= 1 & ,T_{out} &= \frac{1}{T_r}, \\ a_{in} &= \frac{1}{M} & ,a_{out} &= \frac{1}{M\sqrt{T_r}}, \\ \rho_{in} &= 1 & ,\rho_{out} &= \rho_r T_r. \end{aligned} \tag{11}$$

Varying V_{ref} from 0 to 1, the parametrization transitions between right pointing wakes and left pointing jets. Examples of velocity profiles are illustrated in figure 2.

Figure 3 shows a low frequency spatial spectrum for incompressible, isothermal flows, both jets and wakes exhibiting modes matching acoustic duct modes. For low Mach number, acoustic modes become evanescent waves or pseudo-sound, with exponential decay of pressure disturbances [17].

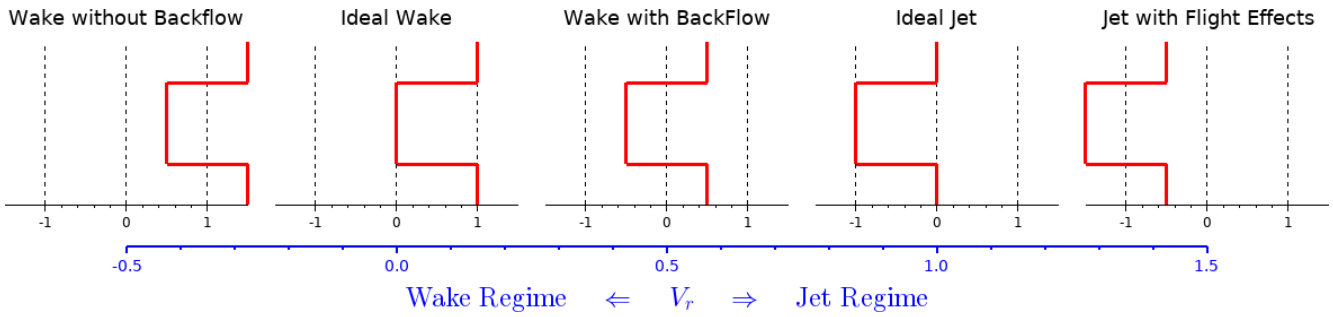

Fig. 2 DVS flows obtained with the parametrization given by equation 11, giving a continuous transition from wakes to left pointing jets.

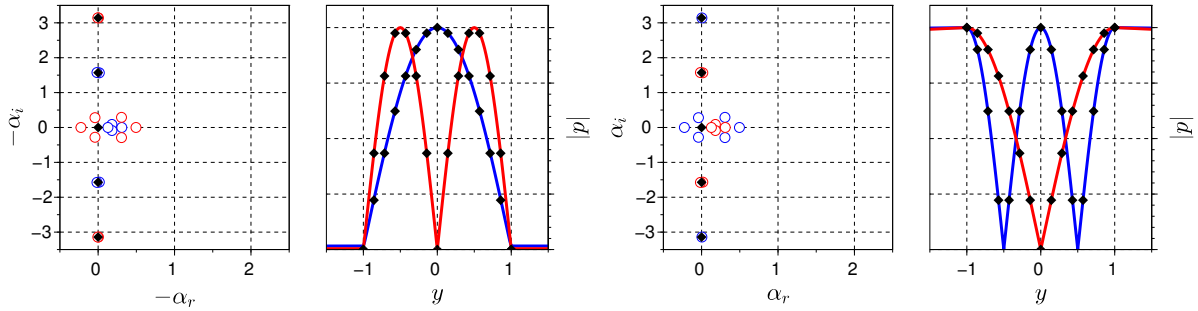

Fig. 3 Comparison between spatial spectrum and mode support of DVS and acoustic duct modes. Results for an ideal jet ($V_{ref} = 1$, left), and wake ($V_{ref} = 0$, right) are compared to soft- and hard-walled ducts, respectively. Circles and solid lines indicate DVS roots and modes ($\alpha \approx -i\pi/2$ and $\alpha \approx -i\pi$) support. Black diamonds mark acoustic-duct modes roots and their spatial support. Red and blue indicate antisymmetric and symmetric modes. Results for a incompressible ($M = 0.01$), isothermal ($T_r = 1$) flow with $\omega = 0.2$.

From equations 8 and 9, low frequencies lead to $c = \omega/\alpha \approx 0$, making the right hand sides small on wakes ($c \approx U_{in}$) and large for jets ($c \approx U_{out}$). The hyperbolic functions on the right will then match the spectrum of acoustic modes, whose modes are separated by $i\pi/2$, with corresponding matching on the modal shapes.

By increasing the frequency, discrepancies between the DVS and acoustic modes are found, as seen Figure 4. These are more pronounced for lower harmonics: as higher harmonics have larger wave-numbers, their phase velocities are smaller, thus satisfying $c \approx 0$ at higher frequencies then lower harmonics.

This result is analogous to Towne at al.'s trapped upstream acoustic waves for $M = 0.9$ jets [12], where total internal reflections were identified as the mechanism behind wave trapping. This mechanism is not present in incompressible flows, and therefore the behavior here discussed must be of a different nature.

The observation that modes for jets and wakes, seen in figure 4, have a qualitative differences, resembling soft- and hard-walled duct modes, respectively, motivates the study of vortex-sheet impedance. As the difference between these ducts lies in the their wall stiffness, vortex sheet impedance, which is a generalized stiffness, can highlight the mechanisms involved in the duct-like behavior of these flows, and their differences.

The vortex-sheet impedance is derived from its definition: the ratio of the inner pressure ($\hat{p}_{in}$) and vertical velocity ($\hat{v}_{in}$), at the interface. For

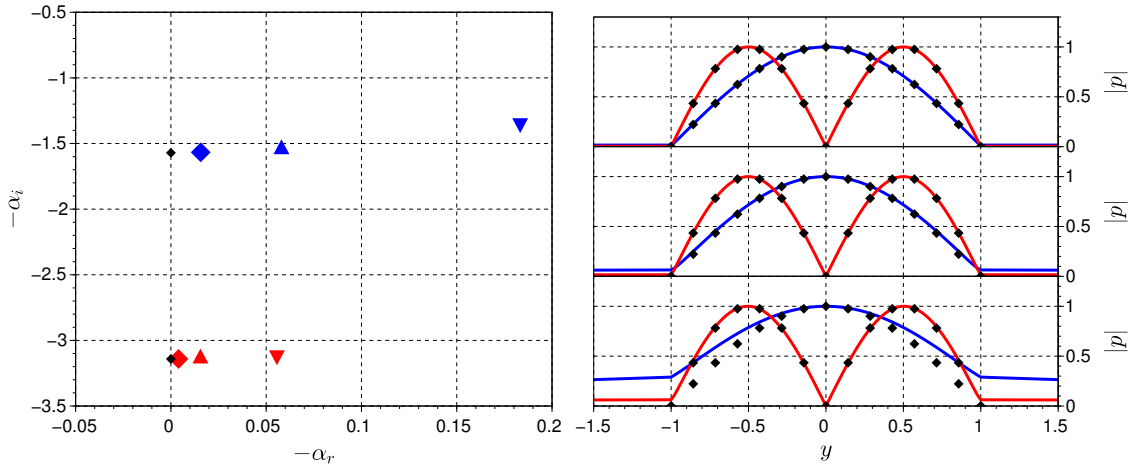

Fig. 4 Spacial Spectrum (on left) and corresponding modes (on right). Blue and red modes correspond to symmetric and antisymmetric DVS modes. Black diamonds represent a soft duct mode. On the left, colored diamonds, upper and lower triangles represents the spatial spectrum for $\omega = 0.2, 0.4$ and 0.8, respectively, with corresponding modes on the right from top to bottom. Parameters used $M = 0.01$, $T_r = 1$. Similar results are found for wakes.

the upper vortex-sheet, using equation 10,

$$Z_{VS} = \frac{\hat{p}_{in}(1)}{\hat{v}_{in}(1)} = \mathrm{i}\alpha(c - U_{in})\frac{\hat{p}_{in}(1)}{d\hat{p}_{in}/dy(1)}. \quad (12)$$

With equations 5–7 an explicit expression is obtained as

$$Z_{VS} = \rho_{out}\frac{\alpha}{\mathrm{i}\xi_{out}}\frac{(c - U_{out})^2}{c - U_{in}}, \quad (13)$$

with an identical expression is found for the lower vortex-sheet.

From the dispersion relations (eq. 8 and 9) we define a reference impedance

$$Z_{ref} = \rho_{in}\frac{\alpha}{\mathrm{i}\xi_{in}}(c - U_{in}), \quad (14)$$

such that the dispersion relations can be written as

$$\tanh(\xi_{in}) = -\frac{Z_{VS}}{Z_{ref}}, \quad \coth(\xi_{in}) = -\frac{Z_{VS}}{Z_{ref}}.$$

The vortex-sheet impedance is large to the reference impedance when $c \approx U_{in}$ and small when $c \approx U_{out}$, explaining why in each of these limits the DVS modes resemble acoustic modes of hard- and soft-walled ducts. The reference impedance, which depends only on the inner region parameters, can be understood as the "strength" of the inner fluid perturbations, to which the "wall" stiffness need to be compared to.

3 Acoustic Modes and Global Instability

To study the relation between the acoustic modes in jets and wakes with the development of absolute instabilities, we use a self-consistency procedure: we assume that acoustic duct modes are present in the flow, calculate the impedance ratio and check if the value obtained is compatible with the duct-like assumption. Noticing that, as seen in figure 4, lower harmonics show larger deviations from the duct-like behavior, we focus the analysis to the first upstream-traveling harmonic on incompressible flows, for which

$$\xi_{in} = -\mathrm{i}\pi/2. \quad (15)$$

Figure 5 shows an impedance map for different values of frequency and V_{ref}, exploring the transition between wakes and jets. At low frequencies, high impedances are found in the wake regime ($V_{ref} \approx 0$) and low impedances on the jet regime ($V_{ref} \approx 1$). Finite values are found in the

transition between these limits and for higher frequencies.

Temperature ratios effects are mapped in figure 6, showing a overall increase in impedance with T_r, improving the duct-like behavior of modes in wakes, while degrading it for jets. This behavior is coincident with the trends obtained by Monkewitz [16]: heating being a instability source for jets, and cooling for wakes. This suggests that the degradation of duct-like behavior might be related to the onset of global instability.

In order to explore this connection we trace the DVS root locus for real frequencies of jets ($V_{ref} = 1$) and wakes ($V_{ref} = 0$) for different temperature rations. Figure 7 shows the formation a saddle point when T_r is varied, formed by a pinching of the KH and acoustic branches, indicating the onset of global instability.

From figure 2, a similar behavior is expected when V_{ref} is varied . By tracing the root locus for different V_{ref}, as seen in figure 8, a similar picture as in 7 is found. The self-consistency condition for the duct-like behavior, is directly related to global instability: its deterioration being a necessary condition to absolute instability, by allowing interactions between acoustic and KH modes.

This results provides an insight on the underpinning instability mechanisms in jets and wakes. Although both systems have been extensively studied in the past decades, to the best of the authors knowledge no clear connection between them has been traced. Monkewitz et al. [11] observed that dispersion is invariant if $U_{in,out}$ and symmetries are exchanged. This results predicts opposite symmetries in their instabilities, but offers little insight on the physical mechanism behind them.

4 Identification of Acoustic Modes in M=0.4 Jet

Once the role of acoustic modes in DVS flows was established, we explore a realistic flow at subsonic Mach number, showing that the results obtained for the incompressible DVS are not an artifact of the model used. Focusing on lower Mach numbers, we bridge Towne et al.'s [12]

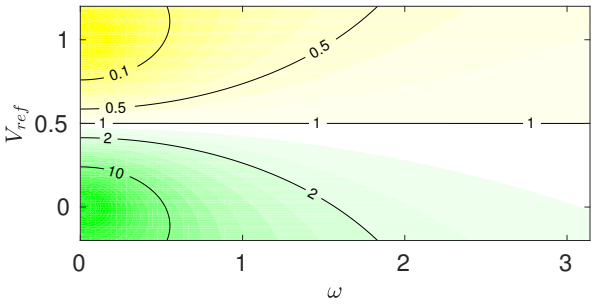

Fig. 5 Impedance ratio ($\mathcal{Z}_{VS}/\mathcal{Z}_{ref}$), as a function of frequency and V_{ref}, on a logarithmic color scale, and values indicated by contour lines. Results for the first upstream-traveling acoustic harmonic for a isothermal ($T_r = 1$) and incompressible ($M = 0.01$) flow.

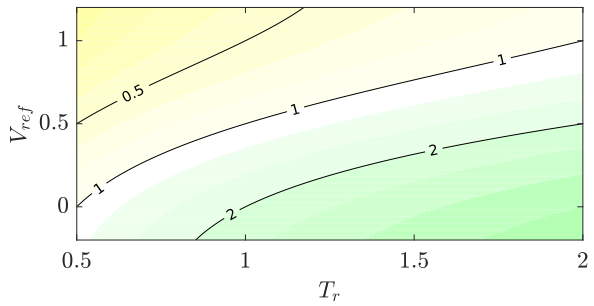

Fig. 6 Same as figure 5, but with $\omega = 0.8$ fixed and varying T_r.

findings for 0.9 Mach jets to the incompressible results presented earlier in this paper. As jets with Mach numbers bellow 0.82 do not sustain total internal reflections, we explore a different flow regime.

We use a Mach 0.4 Jet LES database, detailed in [15], whose mean flow is shown in figure 9. Pressure fluctuations, $p(x,r,\phi,t)$, were decomposed into their azimuthal components

$$p(x,r,\phi,t) = \sum_n p_n(x,r,t)e^{in\pi\phi}. \qquad (16)$$

Unlike Towne et al. [12] and Schmidt et al. [13], there is no visible indications of upstream-traveling modes inside the potential core for the decomposed perturbations. The identification of acoustic modes is then performed via empirical transfer functions [18]. If upstream-traveling acoustic modes are present in the flow, then they

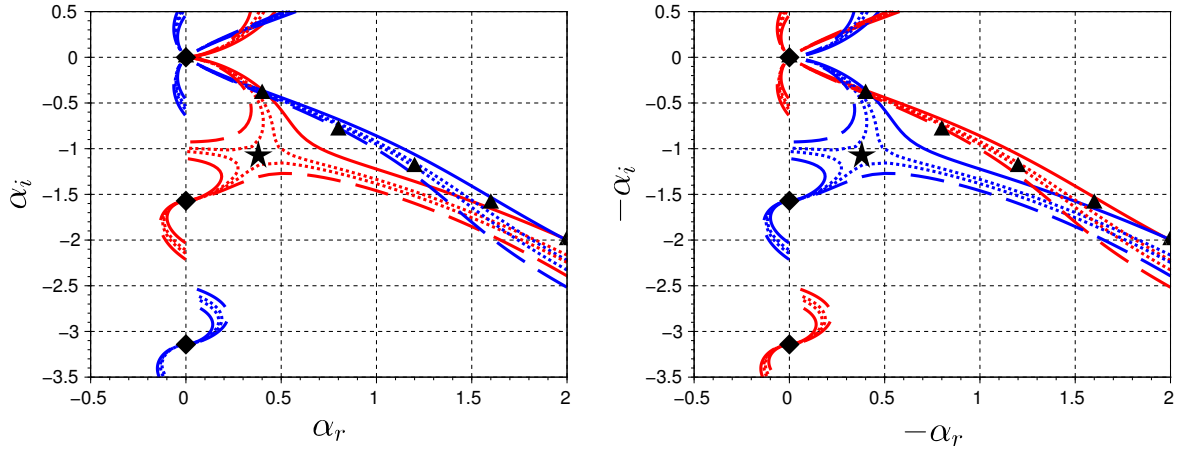

Fig. 7 Spacial spectrum for incompressible ($M = 0.01$) DVS flows, showing the transition from convective to absolute instability, marked by a pinching of KH and acoustic branches. On the left: solid, dotted and dashed lines correspond to $T_r = 1, 0.80/0.76$ and 0.6. Reciprocal ratios $(1, 1.25/1, 28, 1.68)$ are used for the jets on right. Blue/red lines represent antisymmetric/symmetric modes. Diamonds and upper triangles indicate duct and single vortex-sheet modes. The pentagram marks the saddle location in the α plane. Locus for $\omega \in [0, 1.5\pi]$.

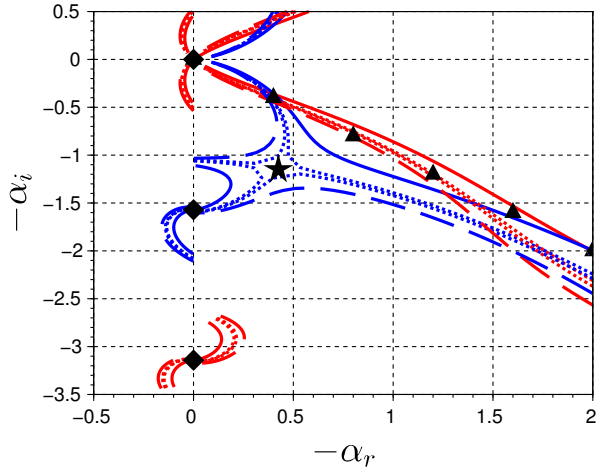

Fig. 8 Same as figure 7, but with solid, dotted and dashed lines representing $V_{ref} = 1, 0.94/0.93, 0.90$.

should be reflected in the transfer function between downstream (input) and upstream (output) points inside the potential core. As these modes are clearly not dominant in jet dynamics, they will only be visible after spurious signals from downstream-traveling modes are filtered out.

The frequency domain transfer function between pressures at $x = 2.0$ and $r = 0$ and the remaining flow field is computed by

$$\tilde{T}_{f,n}(x,y,\omega) = \frac{\langle \tilde{p}_n^+(2,0,\omega)\tilde{p}_n(x,r,\omega)\rangle}{\langle \tilde{p}_n^+(2,0,\omega)\tilde{p}_n(2,0,\omega)\rangle}, \quad (17)$$

where $\langle\cdot\rangle$ denotes averaging and tilde denotes time Fourier transformed quantities and $+$ complex conjugation.

This procedure does not distinguish between causal and non-causal sources: it also contains information of downstream-traveling structures moving from the output to the input positions. We enforce causality from the reference, input, to the output flow fluctuations, which preserves the upstream-traveling acoustic modes and filters out downstream-traveling components, by computing the time domain transfer function,

$$T_{f,n}(x,y,t) = \int e^{-i\omega t}\tilde{T}_{f,n}(x,y,\omega)d\omega, \quad (18)$$

and extracting its causal component ($T^c_{f,n}$),

$$T^c_{f,n}(x,y,t) = T_{f,n}(x,y,t)H(t), \quad (19)$$

where $H(t) = 1$ for $t > 0$ and zero otherwise. Afterwards the causal frequency domain transfer function is obtained,

$$\tilde{T}^c_{f,n}(x,y,\omega) = \frac{1}{2\pi}\int e^{i\omega t}T^c_{f,n}(x,y,t)dt. \quad (20)$$

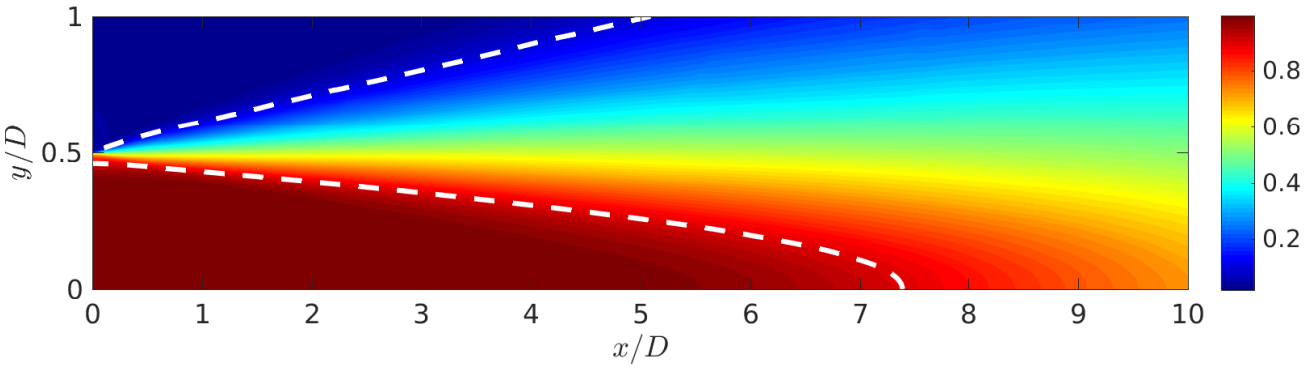

Fig. 9 Mean flow profile for the jet at 0.4 Mach. Color scale indicate axial velocity, white lines indicate velocities equal to 0.1 and 0.9 of the jet velocity.

The transfer function was calculated with a total of 10000 snapshots, with propagative time step of 0.2 between samples. Blocks of 128 snapshots, with 75% overlap were windowed by a Hann function and used for estimating $\tilde{T}_{f,n}(x,y,\omega)$.

Figure 10 shows the asymmetric transfer function ($n=0$) amplitude across the jet center line, $\tilde{T}^c_{f,0}(x,0,\omega)$, for three different frequencies. For these frequencies the decay in amplitude of the transfer function matches the decay of evanescent, upstream-traveling, duct-like acoustic waves, which are given by $e^{\alpha_i x}$, where α_i is the imaginary part of the cylindrical acoustic duct wave number, given by

$$\alpha = -\frac{M\omega \pm \sqrt{\omega^2 - 4\beta_0^2(1-M^2)}}{1-M^2}, \qquad (21)$$

where $\beta_0 = 2.4048$ is the first zero of the Bessel function of the first kind, $J_0(\beta_0) = 0$.

Figure 11 shows the transfer function radial support. The acoustic trend found on the center line is not well recovered around the shear layer, with its radial support showing significant deviations from the expected duct mode counterparts. This deviations are probably due the large difference in amplitude of KH and acoustic modes in the flow, the first being a dominant component of it. The evanescence of acoustic modes makes their signal exponentially small, and spurious KH components modes contaminate the results. This effect is stronger around the shear layer, where acoustic modes have small pressure signals. The increasing dominance of vortex-sheet pressure on points distant from the reference supports this hypothesis.

In spite the feebleness of evanescent acoustic modes in this turbulent flow, the matching between duct acoustic modes decay rate and of the transfer function on the jet centerline indicates that even on absolutely stable flows, non-linear interactions can excite linear acoustic modes in the jet core. Further studies might lead to better ways of filtering out spurious signals.

5 Conclusion

We show that soft-walled duct-like acoustic modes can be found not only in subsonic jets with high Mach number, but also for intermediary Machs and for incompressible flows. The role of these modes in the transition from convective to absolute instability on incompressible flows is presented, showing that the dominant saddle is formed by a pinching of the Kelvin-Helmholtz and upstream-traveling acoustic branches.

Results for incompressible wakes also indicate the presence of acoustic modes, with identical instability role as the incompressible jet. On wakes however, they resemble acoustic modes in hard-walled ducts. The difference in the first acoustic mode harmonics on jets and wakes reflects, and possibly explains, the difference in these flows unstable modes.

The physical mechanism behind the emu-

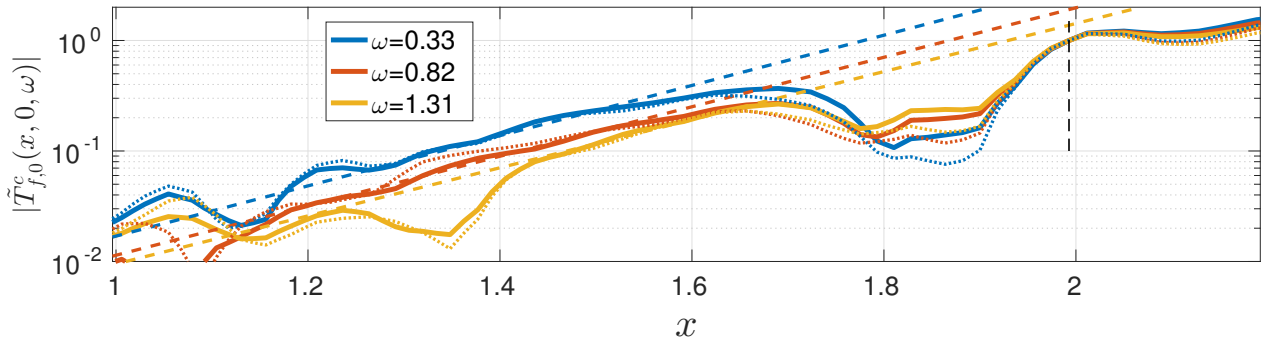

Fig. 10 Transfer function axial support for the first azimuthal pressure distribution along the jet axis. Dashed lines represent transfer function using half of the available data, dotted lines indicate the expected acoustic mode decay, which match the transfer function after a transient distance, possibly related to other faster-decaying modes.

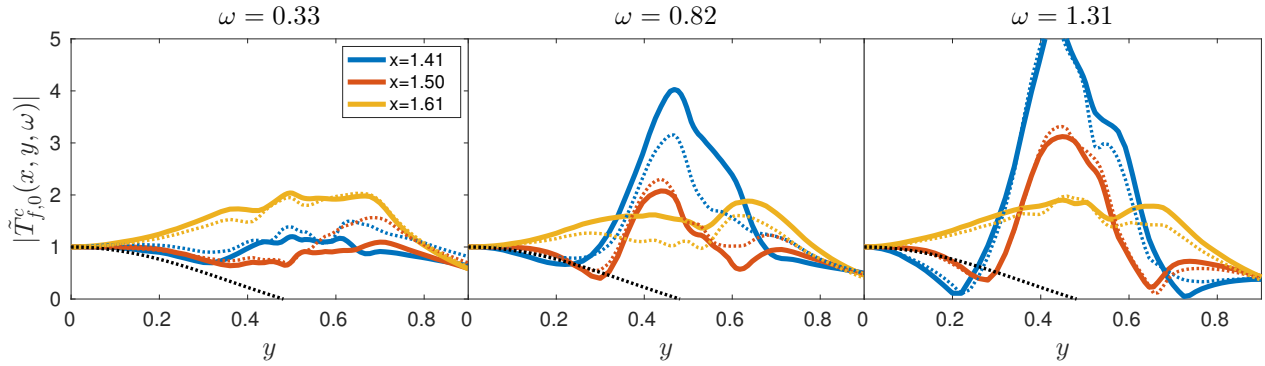

Fig. 11 Transfer function radial support for the first azimuthal pressure distribution, normalized by the transfer function at the centerline, and expected acoustic duct in black. Deviations, particularly around the shear layer ($r = 0.5$), increase for points distant from the reference, indicating bad signal to noise ratios, particularly between acoustic and KH modes.

lation of acoustic duct modes is explained by analyzing the vortex sheet impedance, which shows clear trends of small and large values for low frequency modes of jets and wakes, respectively. These limits explain the symmetry difference of the first harmonic, and a deviation from these limits appears to be a necessary condition for global instability: this deterioration allowing acoustic modes to interact with Kelvin-Helmholtz modes. This condition was observed when the impedance was disturbed by either back-flow or temperature ratio, indicating robustness of the proposition.

With further exploration the concepts detailed in this article, it is possible to explain a larger range of phenomena, which were previously unconnected, with a single framework: the presence of acoustic modes in double sheared flows. Beyond the opposite symmetries of unstable modes on jets and wakes, and destabilization due to back-flow and temperature ratio, it is possible that the different effects of compressibility on jet and wakes instabilities and the appearance of supersonic unstable modes on jets with Mach higher than 2, be explained with similar reasonings. Insights on the mechanisms involved in the destabilization of wakes, but not of jets, due to finite shear layers might be obtained. These possibilities, and possible role of these modes in nonlinear jet dynamics, are currently under study. Understanding the mechanisms behind upstream-traveling modes responsible for global instabilities, might lead to novel passive and active control approaches.

References

[1] Michalke, Alfons, P. On the inviscid instability of the hyperbolic tangent velocity profile *Journal of Fluid Mechanics*, Vol. 19, number 4, pages 543-556, 1964.

[2] Michalke, Alfons, P. Survey on jet instability theory *Progress in Aerospace Sciences*, Vol. 21, pages 159-199, 1984.

[3] Tam, Christopher KW and Hu, Fang Q. On the three families of instability waves of high-speed jets *Journal of Fluid Mechanics*, Vol. 201, pp 447-483, 1984.

[4] Krothapalli A. Discrete tones generated by an impinging underexpanded rectangular jet *AIAA journal*, Vol. 23, number 12, pp 1910-1915, 1985.

[5] Gojon R, Bogey C. Feedback loop and upwind-propagating waves in ideally expanded supersonic impinging round jets *Journal of Fluid Mechanics*, Vol. 823, pp 562-591, 2017.

[6] Gojon R, Bogey C and Marsden, O. Large-eddy simulation of underexpanded round jets impinging on a flat plate 4 to 9 radii downstream from the nozzle *AIAA journal*, Vol. 2210, pp 2015, 2015.

[7] Gojon R, Bogey C. Flow structure oscillations and tone production in underexpanded impinging round jets *AIAA journal*, Vol. 2210, number 6, pp 1792-1805, 2017.

[8] Yamouni S and Sipp D and Jacquin L. Interaction between feedback aeroacoustic and acoustic resonance mechanisms in a cavity flow: a global stability analysis *Journal of Fluid Mechanics*, Vol. 717, pp 134-165, 2013.

[9] Garrido F, Sánchez, E and Buendıa J. Instability Analysis of Incompressible Open Cavity Flows *ETSIAE UPM Madrid*, Vol. 823, pp 562-591, 2014.

[10] Huerre, Patrick and Monkewitz, Peter A Absolute and convective instabilities in free shear layers *Journal of Fluid Mechanics*, Vol 159, pages 151–168, 1985

[11] Monkewitz, Peter A. and Huerre, Patrick and Chomaz, Jean-Marc Global linear stability analysis of weakly non-parallel shear flows *Journal of Fluid Mechanics*, Vol 251, pages 1–20, 1993

[12] Towne, Aaron and Cavalieri, André VG and Jordan, Peter and Colonius, Tim and Schmidt, Oliver and Jaunet, Vincent and Brès, Guillaume A Acoustic resonance in the potential core of subsonic jets *Journal of Fluid Mechanics*, Vol. 825, pages 1113-1152, 2017

[13] Schmidt O, Towne A, Colonius T, Cavalieri A, Jordan P and Brès, G. Wavepackets and trapped acoustic modes in a turbulent jet: coherent structure eduction and global stability. *Journal of Fluid Mechanics*, Vol. 825, pp 1153-1181, 2017.

[14] Jordan, Peter and Jaunet, Vincent and Towne, Aaron and Cavalieri, André VG and Colonius, Tim and Schmidt, Oliver and Agarwal, Anurag Jet-edge interaction tones *arXiv preprint arXiv:1710.07578*, 2017

[15] Schmidt, Oliver T and Towne, Aaron and Rigas, Georgios and Colonius, Tim and Brès, Guillaume A, P. Spectral analysis of jet turbulence *arXiv preprint* , arXiv:1711.06296

[16] Monkewitz P. The absolute and convective nature of instability in two dimensional wakes at low Reynolds numbers. *The Physics of Fluids*, Vol. 31, No. 5, pp 999-1006, 1988.

[17] Hirschberg, Avraham and Rienstra, Sjoerd An introduction to acoustics *Eindhoven university of technology*, Vol. 18, 2004.

[18] Sasaki, Kenzo and Piantanida, Selene and Cavalieri, André VG and Jordan, Peter Real-time modelling of wavepackets in turbulent jets *Journal of Fluid Mechanics*, Vol. 821, pp 458-481, 2017

Copyright Statement